Geophys. J. R. astr. Soc. (1979) 58, 655–666

Regional *S*-wave structure for southern California from the analysis of teleseismic Rayleigh waves

David Hadley and Hiroo Kanamori *California Institute of Technology, Pasadena, California 91125, USA*

Received 1979 January 16; in original form 1978 April 10

Summary. Teleseismic Rayleigh waves, $M_S > 7.0$, in the period range 14 to 28 s, are well recorded by the short-period Benioff array within southern California. Multiple arrivals that hinder the determination of local phase velocity curves are detected by narrow band-pass filtering. The records are then windowed on distinct, coherent peaks that move uniformly across the array. Four to seven stations are included in the determination of both the phase velocity across the array and the incidence azimuth. For earthquakes in the western Pacific, the derived incidence azimuths are systematically rotated counterclockwise by 2–16°. Most of this rotation results from refraction at the continental shelf. Phase velocity data for both the southern Mojave–central Transverse Ranges and the Peninsular Ranges are inverted to obtain regional *S*-wave velocity models. The starting models are constructed from travel-time studies of local sources, both natural and artificial. Poisson's ratio as a function of depth is calculated for these two regions. The comparison of Poisson's ratio with laboratory ultrasonic studies requires a quartz-rich crust within the southern Mojave–central Transverse Ranges and a mafic crust within the Peninsular Ranges.

Introduction

Many investigators are currently pursuing research on such diverse topics as visco-elastic models of the great bend in the San Andreas and the possibly related mechanisms of uplift and deformation; propagation of energy from the seismic source to the free surface; and the quantification and description of the continuing seismicity. These examples and many others all have in common the requirement of an accurate description of the structure of the southern California crust and upper mantle. Multiple *P*-wave travel-time studies from both natural and artificial, local and teleseismic sources have provided significant data on the regional average structure (Gutenberg 1944, 1951, 1952, 1955; Richter 1950; Shor 1955; Press 1956, 1960; Roller & Healy 1963; Kanamori & Hadley 1975). With the rapid growth of the short-period vertical seismic array within southern California, recorded at Caltech in conjunction with the US Geological Survey, average *P*-wave models for individual geologic provinces are becoming available. The relatively coarse nature of these models reflects the

averaging effects of refraction profiles that extend over path lengths of several hundred kilometres. Teleseismic *P*-delay studies, with somewhat better local resolution, have mapped local velocity anomalies within the upper mantle beneath southern California (Raikes 1976; Raikes & Hadley 1978). These studies have demonstrated a remarkable continuity of a mantle *P*-wave velocity anomaly across the San Andreas fault. Observations such as these have major implications for the thickness of the lithosphere and the lateral extent of the boundary between the North American and the Pacific plates (Hadley & Kanamori 1977).

Although the *P*-wave velocity model for southern California is slowly becoming more detailed and precise, the *S*-wave structure has been virtually ignored. There are several obvious reasons for this: first, good *S*-wave travel times are difficult to measure as the initial *S* wave is often obscured by the *P*-wave coda. This is particularly true for the phase that refracts along the top of the mantle, S_n. The arrival most often timed as *S*, even beyond the crossover to S_n, is the phase that propagates at approximately midcrustal velocities, S_g. Secondly, about 95 per cent of the southern California array is devoted to short-period vertical instruments and no *SH* energy is observed. If *SH* energy were observable, the first problem would not be quite as acute. Thirdly, *S* waves are not well excited by artificial sources. The *S* energy observed at stations must typically result from a strong *P*–*S* conversion at some unknown velocity gradient. This uncertainty adds an ambiguity to the origin point and time for the *S* wave. If the first difficulty were not so severe, this complication would be acceptable. We would anticipate mapping at least three branches of the travel-time curve corresponding to the *P*-wave branches of 5.5, 6.1–6.3 and 7.8 km/s.

As suitable refraction data are not readily available, we have designed a technique for deriving local crustal structure that utilizes the dispersion characteristics of fundamental mode Rayleigh waves from distant teleseisms. The teleseisms used in this study are listed in Table 1. Our period range of interest is from 10 to approximately 50 s. However, the bandpass of the presently available data recorded by short-period Benioff instruments limits the data set to periods shorter than 30 s. As we will show later, even this limited band can provide important constraints on the local *S*-wave structure.

The use of the Rayleigh waves in the period range 10–30 s is severely complicated by the effects of multipathing. Unless the effects of this interference can be removed, the data are most often unusable. Capon (1970) has introduced a high-resolution frequency–wavenumber method for handling the problem. This technique requires 'approximately one hour ... (of) ... IBM 360/65' computer time for the analysis of about four periods from one event. Within this study we present a somewhat simpler, and hence less expensive, technique for separating Rayleigh waves that have travelled along multiple paths. Our method relies

Table 1. Locations, dates and magnitudes of the events used in this study.

DATE	LATITUDE	LONGITUDE	M_S	MOJAVE	PENINSULAR
12/15/71	56.0 N	163.2 E	7.8		*
12/2/72	6.4 N	126.6 E	7.4	*	
6/17/73	43.1 N	145.7 E	7.7	*	*
12/29/73	15.1 S	166.9 E	7.2	*	
1/10/74	14.4 S	166.9 E	7.2	*	
10/3/74	12.3 S	77.8 W	7.6		*
5/10/75	38.2 S	73.2 W	7.7	*	*
5/26/75	35.7 N	17.3 W	8.1	*	
7/20/75	6.6 S	155.0 E	7.8	*	

on a careful windowing of the recorded Rayleigh wave. The window characteristics are chosen first by narrow band-pass filtering the records. The width of the window is defined by the location of the minimums that bound distinct peaks in the amplitude envelope that propagate uniformly across the array. The windowed data are then Fourier transformed and the phase velocity and azimuth at each period are computed from the least-squares plane fit to the phase angles. The interference pattern of multiple arrivals can often be identified by rapid changes across the array in the shape of the envelope. The technique is unable to separate unambiguously two arrivals of the same period that arrive simultaneously at the array from two distinct paths. This occurrence is manifest in the analysis by large error bars in the estimated azimuth and unstable estimates of the phase velocity. With these criteria of stable envelope shape across the array and stable azimuth and phase velocity measurements, multiple arrivals were separated in time, for approximately 70 per cent of the earthquakes studies, by several multiples of the period.

The method of using phase velocity as determined from local arrays for the investigation of southern California crustal structure was discussed and used by Press (1956) and Alexander (1963). In these studies three stations and the crest and trough method were employed to define both the azimuth and the phase velocity. The resulting data were compared with a set of standard curves of phase velocity versus crustal thickness. From this relatively simple analysis, good estimates of crustal thickness for various subregions of southern California were obtained. In the present study, we utilize data from 4 to 7 stations, constrain the crustal thickness from previous *P*-wave studies, and then derive regional *S*-wave models. The resolution of this technique is controlled by both the available Rayleigh-wave period range and the physical dimensions of the array. This method has the additional advantage of being applicable to structures with velocity reversals.

Data analysis

The fundamental problem in utilizing short-period Rayleigh waves results from multipathing. In the frequency domain, this interference produces scalloping of the amplitude spectrum. The periodicity of the scallops is controlled by the time separation of the multiple arrivals. The amplitude spectrum suggested to us that a signal processing technique could possibly make use of this periodicity in order to separate the interfering arrivals. Good separation of interfering Rayleigh waves from multiple, closely spaced events has been achieved with the complex cepstrum technique (Oppenheim & Schafer 1975; Tsai 1972). Although this method is most effective when the interfering signals have the same wave shape, tests with chirped sinusoids with slightly different dispersion were quite promising (Linville 1971). Our numerical experiments with simple linear filtering of the cepstrum reproduced both input records. However, tests with real data were rather disappointing. The failure of this technique can be attributed to at least two problems: (1) For the events studied ($M_S > 7.0$), short-period Rayleigh waves arrived at the stations for about 1 hr. Clearly the later phases represent energy that has traversed paths differing substantially from the initial arrivals. These later phases strongly violate the assumption of an approximately stable waveform. Truncation of the data is required, but the location and the manner of this truncation are quite ambiguous. If the truncation is done incorrectly, spurious energy is convolved with that portion of the record which is of most interest. (2) Although the linear filtering of the complex cepstrum for the synthetic data was rather obvious and could have been automated, peaks in the cepstrum of the real data were not distinct and could not be separated. Because of these complications we have abandoned this technique for the present problem.

Our present approach for identifying and separating multiple arrivals relies on narrow band filtering of the data. This technique of separating multiple arrivals is similar to that of

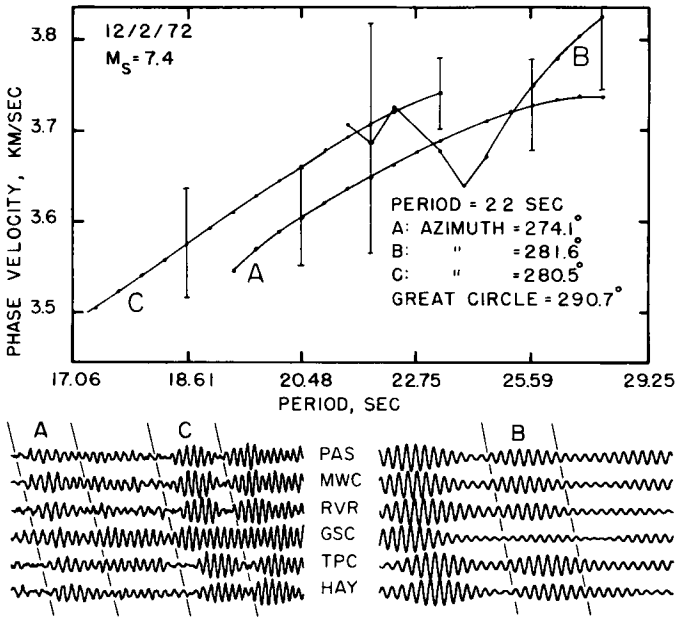

Figure 1. Rayleigh waves recorded across the southern California array for a magnitude 7.4 event in the Philippines. The records at the lower right are narrow band-passed filtered for a period of 25 s. Note the second multipathed arrival. The phase velocity curves derived from the windowed data as shown, and the calculated incidence azimuths, illustrate the extensive multipathing. The duration of the record sections is 12 min.

Pilant & Knopoff (1964). Fig. 1, lower left, shows a good example of the original Rayleigh waves recorded by six stations. The records on the lower right show the same data after processing with a narrow band-pass, zero phase shift filter centred at a period of 25 s. The second arrival, marked 'B', is clearly visible. The window location for processing the original data is selected by bandpass filtering the data with filters that span the range of observable periods and are spaced by about 4 s. The dashed lines in Fig. 1, labelled 'B', indicate a typical window selection. The shape of the window can be used effectively to smooth the Fourier phase spectrum data. Fig. 2 shows a suite of phase velocity curves derived from data selected in a manner identical to that shown in Fig. 1. Before Fourier transforming the data, the amplitude of the front and back portions of the record are smoothly decreased to zero by multiplying by a cosine term. The percentages shown on the curves of Fig. 2 indicate the portion of the record modified by the window. The vertical lines indicate the frequency range of coherent energy as determined from the previous narrow bandpass filtering. Within this frequency range, the derived phase velocity is relatively insensitive to the shape of the window. Outside of this range, the window has the effect of smoothing the phase velocities. For this study, the phase velocity curves have been constructed in sections by overlapping windows. All selected data have been smoothed with a 100 per cent cosine taper. Fig. 1 shows an example of the phase velocity curves derived by this overlap processing technique.

The phase velocity curves are obtained by first Fourier transforming the windowed data. The phase angles that result from this transform are simply related to the phase velocity of the propagating Rayleigh wave. The derived phase angles range between 0 and 2π. For the general case of an array several wavelengths in dimension, an appropriate multiple of 2π must be added to the phase angles to restore the true relative angles. For a wide range of C, such as 3.7 ± 0.4 km/s, and an average station spacing of about one wave-

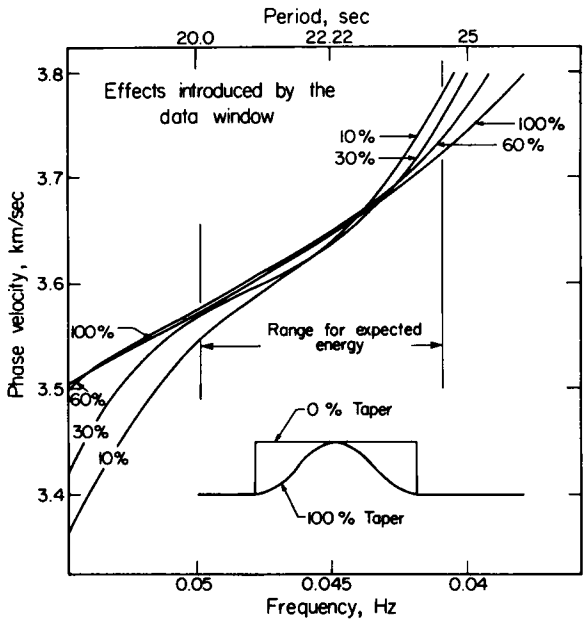

Figure 2. The averaging effect of the cosine taper used to window the data. The percentages shown on the curves indicate the portion of the processed record modified by the window. The vertical lines indicate the range of expected energy as determined from the previous narrow band-pass filtering.

length or less, the appropriate number of multiples of 2π are easily restored to the phase data. Finally, the phase velocity across the array and the azimuth of approach at each frequency step are simple functions of the strike and dip of the plane fitted by least squares to the phase angles from all of the stations (Press 1956; Aki 1961). By using more than three stations, the regression also provides error estimates on the phase velocity and azimuth. We typically use from four to seven stations in the analysis. The final phase velocity curve for each teleseism is finally computed from a range of windowed data that span the frequency band. At each frequency the velocity is a weighted average, weighted by the square of the inverse of the standard deviation of each individual determination.

It is interesting to note in the example considered in Fig. 1 that at the same period, $T = 22$ s, the incidence paths for the three distinct windows are all rotated counterclockwise from the great circle path. For the first arrival, 'A', the rotation is in excess of 16°. These large variations in incidence angles pose a minor problem in regard to the restoration of the 2π multiples to the phase. If the phase is incorrectly restored, the phase velocities and azimuths typically show erratic behaviour between adjacent periods. We have found that a simple search over a range of azimuths, each separated by about 15°, rapidly recovers the true phase.

Fig. 3 illustrates the systematic variation in the observed incidence angles for events around the Pacific. The dark lines represent the great circle azimuths and the light the derived azimuths for the period $T = 20$ s. The systematic counterclockwise deflection is largely controlled by refraction at the continental shelf. The upper part of Fig. 3 plots the calculated phase velocity within the Pacific plate as a function of incidence angle at the continental slope. At large incidence angles the calculated velocity is similar to the velocity of 4.0 km/s determined by Kausel, Leeds & Knopoff (1974) and Forsyth (1975). This suggests that the initial Rayleigh waves detected in southern California traverse the northern Pacific along the great circle path. The calculated high phase velocities for the small

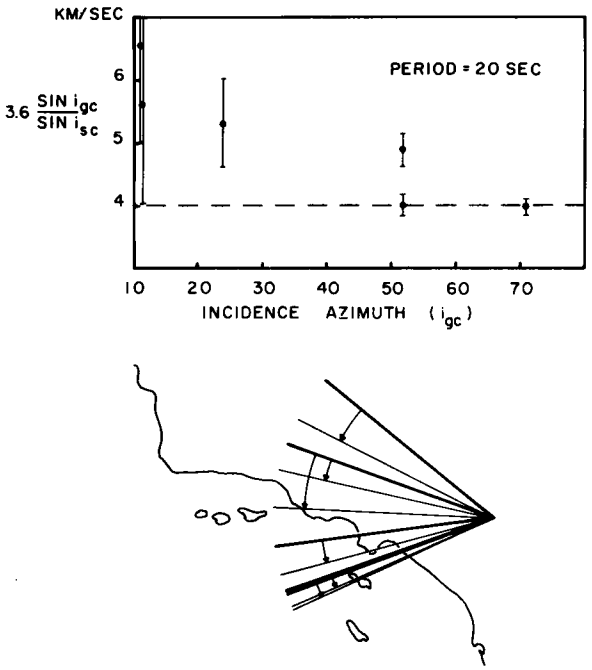

Figure 3. The systematic counterclockwise rotation of the incidence azimuth for earthquakes located around the Pacific. The incidence azimuths were determined from the data recorded by the array shown in Fig. 4. If the deflection is entirely controlled by the continental shelf, the calculated phase velocity for the oceanic crust, $T = 20$ s, computed from the observed phase velocity, azimuth, and expected incidence azimuth at the shelf, should be 4.0 km/s. The deviation from this value for waves crossing the south Pacific suggests a deviation from the great circle path.

incidence angles indicate that either energy crossing the south Pacific deviates from the great circle path by several degrees, or the oceanic–continental transition is not coincident with the continental slope.

The phase velocity curves from the seven teleseisms are plotted in Fig. 4. The inset map shows the station distribution and the measured incident azimuths. The phase velocity data used in the inversion described below were calculated from an average of the individual curves, weighted by the inverse of the standard deviations. The average weighted standard deviation, weighted by the inverse of the standard deviations of the individual determinations, is approximately 0.05 km/s. Data for the inversion were then sampled at a period spacing of 2 s. For the present study these phase velocities provide a good constraint on the regional average S-wave velocities.

The phase velocity curves are inverted with a damped generalized inverse technique (e.g. Franklin 1970; Wiggins 1972). We assume the data and the model are related by:

$$AM = D \tag{1}$$

where M and D are vectors representing, respectively, the desired perturbation to the starting model and the difference between the real and the model data. A is the matrix of partial derivatives that maps M into D. The model is then calculated using:

$$M = A^{\mathrm{T}}(AA^{\mathrm{T}} + (r/(1-r))V)^{-1}D. \tag{2}$$

The range of r extends from 0 to 1. This variable controls the stability of the solution. Clearly, as r tends to zero, the solution moves smoothly to the undamped inverse. The

matrix V is the data variance matrix. The diagonal elements are the variance of each determination of the phase velocity. The off-diagonal terms describe the covariance between different frequencies. Because of the window characteristics used in the data processing, the covariance terms are not all zero. However, the covariance between periods at opposite ends of the frequency band is near zero. We therefore have tapered the covariance matrix with a Gaussian function to approximate the data smoothing inherent in the processing. Finally, the averaging kernel for layer i is given by:

$$F_i = A^{\mathrm{T}}(AA^{\mathrm{T}} + (r/(1-r))V)^{-1}AE_i \tag{3}$$

where E_i is the unit vector in the ith direction. The averaging kernel describes the resolution of the derived model.

The geographical region shown in Fig. 4 is essentially the same as that previously studied by Kanamori & Hadley (1975). In that study about 20 quarry blasts were used to determine an average P-wave crustal structure. For the inversion of the data shown in Fig. 4, the starting model was modified from the earlier study. The 6-km thick upper layer was divided into a 1-km low-velocity surface layer, $V_P = 3.5$ km/s, and a second layer with $V_P = 5.5$ km/s. The 21-km thick, $V_P = 6.3$ km/s layer was subdivided into four layers. The rest of the model was unchanged. The S-wave velocity for the starting model was calculated from the P-wave model with the assumption of Poisson's ratio of 0.25.

An examination of the layer partial derivatives in the A matrix indicates that except for the shallow crustal layers the S-wave partial derivatives are several times larger than those for P waves. This means that perturbations to the model occur primarily in the S-wave structure. Because of this insensitivity to P-wave structure, we have inverted the phase velocity data with several different P-wave starting models. The range of P-wave models employed in the inversion actually extend beyond the limits imposed by the quarry blasts travel-time data. The velocity limits shown in Fig. 4 bound all S-wave models that resulted from the various inversions. The averaging kernels indicate that the derived layer velocities actually represent

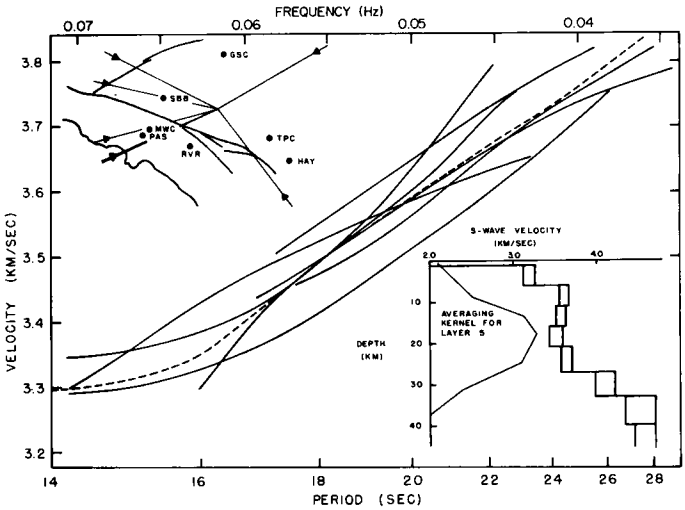

Figure 4. Phase velocity dispersion curves for the Mojave region, the stations used, azimuth of approach for the seven events analysed, and the S-wave crustal model derived from the inversion of the dispersion curves. The dashed curve is the weighted average phase velocity curve. The bounds on the model are maximum and minimum models derived from a wide range of starting models. A mid-crust low-velocity zone is suggested by all inversions; however, the resolution is not sufficient to require this feature. The averaging kernel for layer 5 is inset with the model.

weighted averages of the adjacent model layers, the weighting function being the averaging kernel. The combination of the *P*-wave data from the quarry blasts and the phase velocity data requires a model at least as complex as that shown in Fig. 4.

Through all the inversions an average high-velocity layer was required at the base of the crust, $V_S = 4.1$ km/s. This result is similar to that derived from the previous *P*-wave velocity studies. The Moho reflection, P_MP, was observed to be critically reflected at a distance, Δ_c, of 90 to 98 km. Combined with good data for the upper crust and the P_n velocity of 7.8 km/s, the observed Δ_c required a high-velocity layer at the base of the crust (Kanamori & Hadley 1975).

The inversion of the phase velocity data suggested an additional interesting complication. All *S*-wave models, originating from rather diverse starting models, have a mid-crustal, layer 5, low-velocity zone. The velocity contrast between layer 3, typically the fastest overlying layer, and layer 5, ranges from 0.1 to 3 per cent. The depth to this possible velocity reversal is similar to the thickness of the seismic zone within southern California. These results are very similar to those of Keller, Smith & Braile (1975) and Bache, Rodi & Harkrider (1978) for profiles in the adjacent Basin and Range province. Unfortunately, the limited frequency band of the phase velocity data does not provide sufficient information to resolve this feature. The resolution and possible lateral variation of a crustal low-velocity zone, and its influence, if any, on the depth of the seismic zone within southern California, will require studies that employ small, dense arrays of broad-band instruments.

The previously discussed, averaged model for the southern Mojave and the central and eastern Transverse Ranges (Kanamori & Hadley 1975) has been a useful model for location and focal mechanism studies of earthquakes recorded by the regional array. A similar, average model appears useful for continuing studies within the Peninsular Ranges of southern California. Toward this goal, we have collected travel-time data from several natural and artificial sources, determined the Rayleigh wave phase velocity curves as discussed above, and surveyed previous geophysical studies of the province. The first and most obvious conclusion of this study is that most physical parameters of the province have large lateral variations. An east–west profile of the depth to the Moho through the latitude of the Salton Sea would show a crustal thickness of 20–25 km in the adjacent continental borderlands (Shor & Raitt 1956), a relatively smooth increase to 30–35 km beneath the centre of the range, and a rapid decrease to possibly less than 20 km beneath the Salton Sea. The *P*-wave velocities in general show similar variations. The shallow upper crust varies from 5.8 km/s in the north to 6.4 km/s (Simons 1977) in the south. The east–west lateral changes are equally severe, with velocities increasing to the west. The details of the multiple profiles crossing this province and of other profiles within southern California will be published in a separate paper. A simple, regionally averaged model based on the compilation of these profiles is presented in Fig. 5. The velocity profile presented by Shor & Raitt (1956) for the north-central portion of the province is shown for comparison. The slightly higher velocities are the result of the southern high-velocity crust.

We have attempted to derive an average Rayleigh wave phase velocity curve for the province, period range of 14 to 26 s. The available stations are shown in Fig. 6. The station distribution, the lateral heterogeneity and the timing resolution prevent the utilization of the teleseisms that arrive at an incidence angle normal to the north-west structural grain of the province. Unfortunately this means that surface waves appropriate for studying the province propagate along paths parallel to the continental shelf. The resulting records are severely multipathed and difficult to use.

Fig. 6 shows the station distribution, incidence azimuths and phase curves derived from four teleseisms. Because of the unfavourable geometry of the array and the lateral

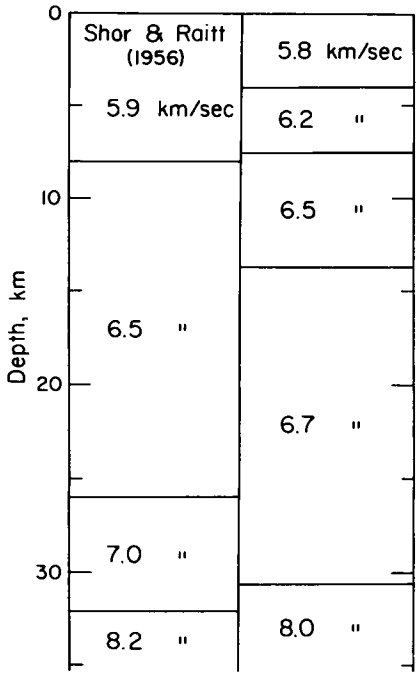

Figure 5. Regionally averaged *P*-wave model for the Peninsular Ranges north of the international border. The model of Shor & Raitt (1956) for the northern portion of the province is shown for comparison. The slightly higher velocities in the average model reflect contributions from the southern high velocity crust.

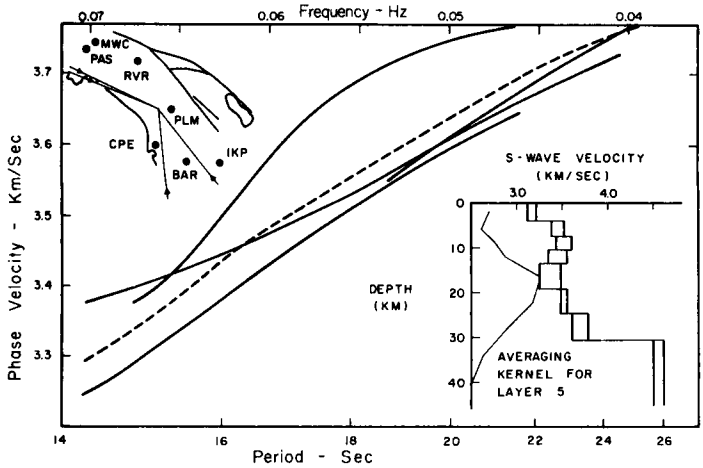

Figure 6. Phase velocity dispersion curves for the Peninsular Ranges, the stations used, azimuth of approach for four events analysed, and the *S*-wave crustal model derived from the inversion of the dispersion curves. The dashed curve is the weighted average phase velocity curve. The bounds on the model are maximum and minimum models derived from a wide range of starting models.

heterogeneity, the weighted standard deviation of the weighted average phase velocity curve is 0.08 km/s. The inversion of the phase velocity data, starting from a range of *P*-wave models as discussed above, results in a fairly simple regionally averaged *S*-wave model, Fig. 6. As in the Mojave region, the various inversions suggested a midcrustal *S*-wave low-velocity

Table 2. V_P, V_S and Poisson's ratio as a function of rock type, confining pressure = 4 kb. The last column contains values of σ corrected to a temperature of 290°C.

Rock	Density	V_p	V_s	σ		σ(T = 290°C)	Ref.
Stirling quartzite	2.495	4.71	3.00	.159		.152	1
Granite, Stone Mt., Ga.	2.639	6.27	3.74	.224		.217	2
Texas gray granite	2.609	6.25	3.61	.227		.227	3
Woodbury granite	2.634	6.29	3.67	.236		.234	3
Granite, Barre, Vt.	2.655	6.25	3.64	.243		.236	2
Granite, Rockport, Mass.	2.638	6.39	3.68	.252		.245	2
Westerly granite	2.63	6.09	3.50	.254		.247	1
Climax stock granodiorite	2.665	6.31	3.53	.273		.266	1
Basalt	2.586	5.80	3.27	.274		.274	3
Hornblend gabbro	2.933	6.86	3.71	.289		.289	3
Bytownite gabbro	2.885	6.81	3.53	.309		.309	3
San Marcos gabbro	2.993	7.01	3.52	.329		.329	3
Eclogite, Headlsburg, Ca.	3.444	8.01	4.58	.257	(10 KB)		2
Periodtite, Hawaii							
#1	3.29	8.21	4.49	.287	"		4
#2	3.29	8.36	4.68	.272	"		4

References:

1 Shock, Bonner & Louis (1974). 2 Press (1966). 3 Hughes & Maurette (1957). 4 Christensen (1966).

zone. However, within the uncertainty in the data, the phase velocities can be matched without this feature. Unlike that from the Mojave, these data do not require a thin, high-velocity, 4.1 km/s layer or transition zone at the base of the crust.

The *P*-wave models for the mid and upper crust for the Mojave and the Peninsular Ranges are quite distinct, in contrast to the *S*-wave models, which are all remarkably similar. This regional variation in the ratio V_P/V_S requires a major change in lithology between the two provinces. The *P*-wave upper crustal velocities in the Mojave, 6.1 to 6.3 km/s, are comparable with those from ultrasonic laboratory measurements on granites, Table 2. The average *P*-wave velocities within the Peninsular Ranges, 6.5 to 6.7 km/s, are indicative of more mafic rocks such as gabbro and diorite. This is consistent with the known surface geology. The Mojave region contains many plutons of quartz monzonite. Plutons within the Peninsular Ranges grade from granodiorite to gabbro. Additional support for the continuation of the surface geology to the mid and lower crust is provided by Poisson's ratio, which is sensitive to composition of the crustal rocks. Table 3 shows values of Poisson's ratio derived from both the *P*- and *S*-wave velocities for several depths. A comparison of these values with measured ratios, Table 2, is consistent with major crustal compositional differences between the two provinces. The observed Poisson's ratio requires a mafic crust for the Peninsular Ranges and a more quartz-rich crust for the southern Mojave and the central Transverse Ranges.

Conclusions and results

(1) Narrow band filtering can identify multiple Rayleigh wave arrivals from teleseisms. Careful windowing of the data, from four or more stations, can provide good estimates of the phase velocity, the incidence azimuth and the respective error estimates.

Table 3. Poisson's ratio for the southern Mojave and Peninsular Ranges.

Depth	Peninsular ranges	Mojave
5	0.287 ± 0.024	0.244 ± 0.031
10	0.295 ± 0.028	0.246 ± 0.027
28	0.280 ± 0.028	0.220 ± 0.040
35	0.269 ± 0.020	0.251 ± 0.025

(2) Incidence azimuths for the first arrival, $T = 20$ s, for events located in the western Pacific, are systematically rotated counterclockwise from the great circle path. A large part of the rotation results from refraction at the continental margin. Rayleigh waves from the south Pacific deviate from the expected azimuth by $1-4^{\circ}$. This may result from either a deviation of the surface waves from the great circle path or from slight non-alignment of the continental slope and the oceanic–continental transition.

(3) Fundamental mode Rayleigh-wave phase velocity curves, $T = 14$ to 28 s, have been measured for both the southern Mojave–central Transverse Ranges and the Peninsular Ranges.

(4) The phase velocity data have been inverted with a damped generalized inverse. The *P*-wave starting models span and extend slightly beyond the limits imposed by quarry blast data. The resulting range of *S*-wave models, Figs 4 and 6, represents the simplest models consistent with the data. All inversions suggest a mid-crustal low-velocity zone that is comparable in depth with the bottom of the seismic zone. However, the accuracy of the present data does not require this feature.

(5) The *P*-wave velocities determined from natural and artificial sources, and Poisson's ratio derived from both the *P*- and *S*-wave velocities, Table 3, require a quartz-rich crust within the southern Mojave–central Transverse Ranges and a mafic crust within the Peninsular Ranges. Both observations are consistent with the surface geology.

Acknowledgments

We thank Dave Harkrider for the computer program used to calculate the layer partial derivatives, and D. Forsyth, R. Mitchel and J. Dewey for critically reviewing the manuscript. This work was sponsored by the USGS under Contract Nos 14-08-0001-15893 and 14-08-0001-16711.

Contribution No. 3054 of the Division of Geological and Planetary Sciences, California Institute of Technology, Pasadena, California 91125, USA.

References

Aki, K., 1961. Crustal structure of Japan from the phase velocity of Rayleigh waves, *Bull. Earthq. Res. Inst., Tokyo*, **39**, 249–277.

Alexander, S. S., 1963. Surface wave propagation in the western United States, *PhD thesis*, California Institute of Technology.

Bache, T. C., Rodi, W. & Harkrider, D., 1978. Crustal structure inferred from Rayleigh wave signatures from NTS explosions, *Bull. seism. Soc. Am.*, **68**, 1399–1414.

Capon, J., 1970. Analysis of Rayleigh wave multipath propagation at LASA, *Bull seism. Soc. Am.*, **60**, 1701–1731.

Christensen, N. I., 1966. Elasticity of ultrabasic rocks, *J. geophys. Res.*, **71**, 5921–5931.

Forsyth, D. W., 1975. The early structural evolution and anisotropy of the oceanic upper mantle, *Geophys. J. R. astr. Soc.*, **43**, 103–162.

Franklin, J. N., 1970. Well-posed stochastic extension of ill-posed linear problems, *J. Math. Anal. Appl.*, **31**, 682–716.

Gutenberg, B., 1944. Travel times of principal *P* and *S* waves over small distances in southern California, *Bull. seism. Soc. Am.*, **34**, 13–32.

Gutenberg, B., 1951. Revised travel times in southern California, *Bull. seism. Soc. Am.*, **62**, 427–439.

Gutenberg, B., 1952. Waves from blasts recorded in southern California, *Trans. Am. Geophys. Un.*, **33**, 427–431.

Gutenberg, B., 1955. Wave velocities in the earth's crust, *Geol. Soc. Am. Special Paper*, **62**, 19–34.

Hadley, D. & Kanamori, H., 1977. Seismic structure of the Transverse Ranges, California, *Geol. Soc. Am.*, **88**, 1469–1478.

Hughes, D. S. & Maurette, C., 1956. Variation of elastic wave velocities in granites with pressure and temperature, *Geophys.*, **21**, 277–284.

Hughes, D. S. & Maurette, C., 1957. Variation of elastic wave velocities in basic igneous rocks with pressure and temperature, *Geophys.*, **22**, 23–31.

Kanamori, H. & Hadley, D. M., 1975. Crustal structure and temporal velocity change in southern California, *Pageoph*, **113**, 257–280.

Kausel, E. G., Leeds, A. R. & Knopoff, L., 1974. Variations of Rayleigh wave phase velocities across the Pacific Ocean, *Science*, **186**, 139–140.

Keller, G. R., Smith, R. B. & Braile, L. W., 1975. Crustal structure along the Great Basin–Colorado plateau transition from seismic refraction studies, *J. geophys. Res.*, **80**, 1093.

Linville, A., 1971. *Rayleigh-wave multipath analysis using a complex cepstrum technique*, Texas Instruments Incorporated.

Oppenheim, A. V. & Schafer, R. W., 1975. *Digital Signal Processing*, Prentice-Hall, Inc., Englewood Cliffs, New Jersey.

Pilant, W. L. & Knopoff, L., 1964. Observations of multiple seismic events. *Bull. seism. Soc. Am.*, **54**, 19–39.

Press, F., 1956. Determination of crustal structure from phase velocity of Rayleigh waves, Part I: Southern California, *Bull. Geol. Soc. Am.*, **67**, 1647–1658.

Press, F., 1960. Crustal structure in the California–Nevada region, *J. geophys. Res.*, **65**, 1039–1051.

Press, F., 1966. Seismic velocities, in *Handbook of Physical Constants*, pp. 195–218, ed. Clark, S. P., Geological Society of America Memoir 97.

Raikes, S., 1976. The azimuthal variations of teleseismic *P*-wave residuals for stations in southern California, *Earth planet. Sci. Lett.*, **29**, 367–372.

Raikes, S. & Hadley, D., 1979. The azimuthal variation of teleseismic *P*-residuals in southern California: implications for upper mantle structure, *Tectonophys.*, submitted.

Richter, C. F., 1950. Velocities of *P* at short distances, *Bull. seism. Soc. Am.*, **40**, 281–289.

Roller, J. C. & Healey, J. H., 1963. Seismic-refraction measurements of crustal structure between Santa Monica Bay and Lake Mead, *J. geophys. Res.*, **68**, 5837–5848.

Shock, R. N., Bonner, B. P. & Louis, H., 1974. *Collection of ultrasonic velocity data as a function of pressure for polycrystalline solids*, Lawrence Livermore Laboratory.

Shor, G. G., 1955. Deep reflections from southern California blasts, *Trans. Am. geophys. Un.*, **36**, 133–138.

Shor, G. G. & Raitt, R. W., 1956. Seismic studies in the southern California continental borderlands, *International Geological Congress, 20th, Mexico*, Trabajos seccion 9, t. 2, pp. 243–259.

Simons, R., 1977. Seismicity of San Diego, 1934–1974, *Bull. seism. Soc. Am.*, **67**, 809–826.

Tsai, Yi-Ben, 1972. Use of *LP* surface waves for source characterizations, *Geophys. J. R. astr. Soc.*, **31**, 111–130.

Wiggins, R. A., 1972. The general linear inverse problem: implication of surface waves and free oscillations for earth structure, *Rev. Geophys. Space Phys.*, **10**, 251–285.